Investigation of mechanical behaviour of non-persistent jointed blocks under uniaxial compression

Mostafa Asadizadeh[*1,2], Mahdi Moosavi[2a] and Mohammad Farouq Hossaini[2b]

[1]*Department of Mining Engineering, Hamedan University of Technology, Mardom Street, Hamedan, 65155-579, Iran*
[2]*School of Mining Engineering, College of Engineering, University of Tehran, 1439957131 Tehran, Iran*

Abstract.   This paper presents the results of an empirical study in which square rock-like blocks containing two parallel pre-existing rough non-persistent joints were subjected to uniaxial compression load. The main purpose of this study was to investigate uniaxial compressive strength and deformation modulus of jointed specimens. Response Surface Method (RSM) was utilized to design experiments and investigate the effect of four joint parameters, namely joint roughness coefficient (JRC), bridge length (L), bridge angle (γ), and joint inclination (θ). The interaction of these parameters on the uniaxial compressive strength (UCS) and deformation modulus of the blocks was investigated as well. The results indicated that an increase in joint roughness coefficient, bridge length and bridge angle increased compressive strength and deformation modulus. Moreover, increasing joint inclination decreased the two mechanical properties. The concept of 'interlocking cracks' which are mixed mode (shear-tensile cracks) was introduced. This type of cracks can happen in higher level of JRC. Initiation and propagation of this type of cracks reduces mechanical properties of sample before reaching its peak strength. The results of the Response Surface Methodology showed that the mutual interaction of the joint parameters had a significant influence on the compressive strength and deformation modulus.

Keywords: physical model; non-persistent joint; mechanical behavior; joint roughness coefficient

1. Introduction

Rock mass is a discontinuous medium with fissures, fractures, joints, bedding planes, and faults. Pre-existing non-persistent discontinuities in rock mass strongly affect initiation and propagation of new cracks. Underground or surface excavation usually disturbs original stability of rock mass. Redistribution of rock mass stress field can trigger new cracks to initiate at or near the tips of pre-existing cracks and propagate toward the direction of the major principal stress, sometimes coalescing with other cracks. The mechanical behavior of rock mass is mainly governed by the behavior of non-persistent discontinuities or planes of weakness. Reliable characterization of mechanical behavior of jointed rock mass is very crucial in safely designing open pit mine slopes and civil structures such as arch dams, bridge piers, tunnels and high slopes. The influence of non-persistent joints on slope stability is illustrated in Fig. 1. These pictures show step-path failure of a slope as a function of non-persistent joints, in an open pit mine and a hydroelectric station. In this issue, mechanical properties of rock bridges and distribution of joints are crucial factors (Huang *et al.* 2015).

The most important characteristics of a rock mass are compressive strength and deformability which represents its mechanical behavior. Estimation of these parameters is somehow complicated. This complexity increases for non-persistent joints due to the interaction of bridges on the strength and failure mode. A substantial number of investigations have focused on mechanical behavior of persistent jointed rocks (Amadei and Goodman 1981, Asadollahi *et al.* 2010, Bahaaddini *et al.* 2015, Bahaaddini *et al.* 2016b, Bahaaddini *et al.* 2014b, Bahaaddini *et al.* 2013a, Einstein *et al.* 1983, Grasselli 2006, Jade and Sitharam 2003, Lajtai 1969a, Li *et al.* 2017, Li *et al.* 2016, Mas Ivars *et al.* 2011, Saeb and Amadei 1992, Serrano *et al.* 2014, Sherpa *et al.* 2013, Wang and Huang 2009, Zhang 2010). While according to Bahaaddini *et al.* (2016a), non-persistent jointed rocks have received less attention mainly due to complex interactions of intact-rock bridges and joints. The coupled effect of joints and intact bridges on mechanical response of rock mass is not clear yet, and this issue is still an open question. An analytical approach was applied to predict the behavior of a rock mass crossed by non-persistent joints, which was based on limit equilibrium method and Mohr-Coulomb criteria (Jennings 1970). Rock mass strength was computed from the simple algebraic weighing of the bridge shearing and sliding along the joints in planar failure mode. Jennings's approach assumed uniform stress distribution over joints, and didn't take into account crack interactions and stress concentration at the crack tips.

An analytical model was presented based on tensile

∗Corresponding author, Ph.D.
  E-mail: m.asadizadeh@hut.ac.ir
[a]Ph.D.
  E-mail: mmoosavi@ut.ac.ir
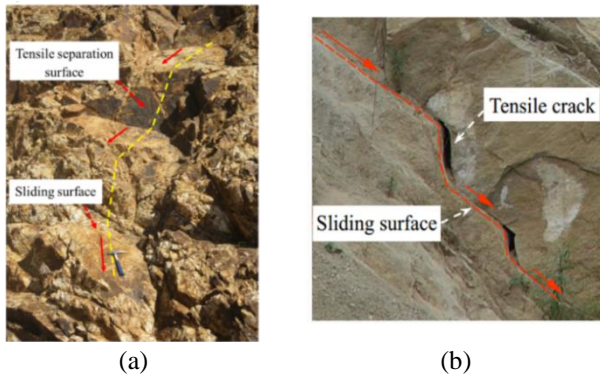[b]Ph.D.
  E-mail: mfarogh@ut.ac.ir

Fig. 1 Non-persistent joints (a) Open pit slope, Daralou copper mine, Iran (b) The reservoir slope of a hydroelectric station (Huang *et al.* 2015)

strength of rock material (Jamil 1992, Cording and Jamil 1997). In this model, tensile failure of bridges and sliding along the joints were assumed and dilatation of joint surface was taken into consideration. Inability to predict mixed mode and pure shear mode of bridge failure is the most important shortcoming of this approach. It can be inferred that analytical methods cannot cover all failure patterns of bridge. Therefore, physical modeling is one of the common ways to investigate the non-persistent jointed rock mass behavior. It is abundantly clear that the bridge angle and bridge length significantly affect the stress distribution, strength and deformation of materials. The effect of non-persistent discontinuities has been investigated in a small number of laboratory experiments on artificial rock-like materials in order to understand the complicated mechanical behavior of non-persistent jointed rock masses (Ashby and Hallam 1986, Van Sint Jan and Prudencio 2003, Mughieda *et al.* 2004, Prudencio and Van Sint Jan 2007, Prudencio 2009, Yang *et al.* 2015, Huang *et al.* 2015, Asadizadeh *et al.* 2017).

A model was developed to predict the growth and interaction of cracks in brittle solids under compressive stress (Ashby and Hallam 1986). The results showed that crack initiation and propagation were controlled by initial crack length and orientation, coefficient of friction and stress state. Sint Jan *et al.* (2003), investigated the strength characteristics of non-persistent joints and described the conditions under which new tensile cracks generate and propagate to connect existing joints so that the rock mass becomes fractured into several blocks, leading to a low strength. The failure mechanisms of joints and bridges in jointed rock masses using a series of uniaxial compression tests were studied and the coalescence path was found to be mainly dependent on the inclination of the bridge between the cracks (Mughieda *et al.* 2004). Moreover, mechanical behavior of non-persistent jointed rock masses using biaxial tests was investigated by [28, 29]. The failure modes and maximum strengths found to be dependent on the geometry of the joint systems, the orientation of the principal stresses, and the ratio between intermediate stress and intact material compressive strength. Yang *et al.* (2015) reported that the peak strength of samples depended on the bridge angle, but the deformation modulus was not closely related to the bridge angle. Investigation of cylindrical rock-like material

by (Huang *et al.* 2015) showed that the peak strength and Young's modulus of pre-fissured specimen containing two unparalleled flaws decreased from flaw angle 0° to 15° and increased from flaw inclination 15° to 70°.

It is clear that, a joint surface naturally has specific JRC. The impact of JRC and its interaction with the other parameters on mechanical response of non-persistent jointed rock blocks have barely been studied. In this paper, mechanical behavior of non-persistent jointed samples containing two parallel (stepped and coplanar) pre-existing mate non-persistent joints subject to uniaxial compression has been studied utilizing physical modeling. To that end, a suitable material was produced and a molding cast was designed to create close non-persistent joints with specific JRC. In order to design the experiments, Response Surface Method was employed. Consequently, the effects of joint roughness coefficient, bridge length, bridge angle, joint inclination and their interactions on the uniaxial compression strength and deformation modulus of the jointed block were studied.

2. Testing material and equipment

2.1 Model material

In this study an appropriate artificial material was designed using plaster, cement, water and some additives. Repeatable tests require a uniform, identical and homogenous specimen. The most important specifications of this material are brittleness, relatively long gelation time and relatively high strength. However, it is common to use a combination of plaster and cement as a model material to simulate a weak rock. This mixture has been utilized because of its instant hardening, flexibility, low cost, easy casting, and availability (Ghazvinian *et al.* 2012 and 2013). Furthermore, higher unconfined compressive strength of this material in relation to pure plaster or pure cement makes it a favorable mix for modeling a jointed weak rock.

2.1.1 Small scale sample preparation

Here, a mixture of plaster and cement type II (40% water and 60% solid) is used to prepare artificial samples. The plaster content (P) is varied from 0 to 60% of solid and cement percent (C) from 60 to 0%, simultaneously. The specimens were prepared by pouring the mixture into the molds. The mould is a split tube with the inner-diameter of 54 mm and height of 160 mm, fastened by connectors. Its base is adhered to a steel plate (Fig. 2(a)). The mold was vibrated in a shaking table for approximately 2 minutes to achieve appropriate compaction and not to form air bubbles. The samples were cut in length of 120±1 mm and then were kept in a room with constant temperature of 25°C from 1 to 28 days depending on the sample objective (Fig. 2(b)).

2.1.2 Optimum mixture plan

In order to optimize the plaster and cement content in the mixture, the variation of material content was considered with plaster content (i.e., P-0% means P=0%, C=60% and W=40%). To do that, 35 samples with five levels of plaster content (0, 10, 20, 30, 40, 50, and 60%)

were examined in 1, 3, 7, 14 and 28 days. The UCS tests were done according to ASTM (D2938-95) and using a loading frame. The effect of plaster and cement content on unconfined compressive strength of prepared samples at different ages is presented in Fig. 3.

(a) (b)

Fig. 2 The preparation of samples using the mold, (a) The mold of sample preparation and (b) The prepared samples
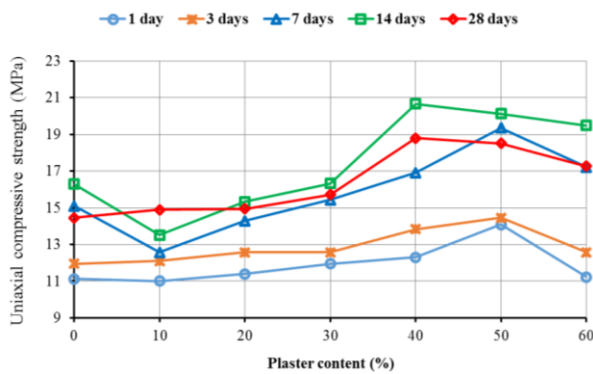

Fig. 3 The effect of the plaster/cement content on UCS of samples with different ages
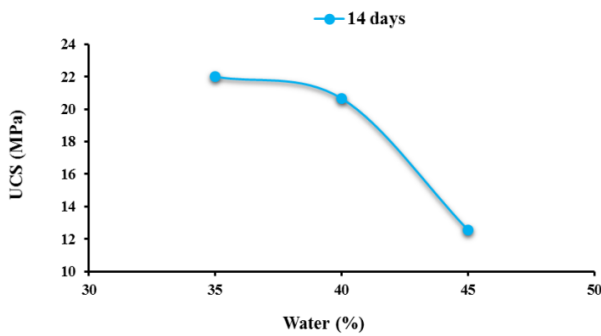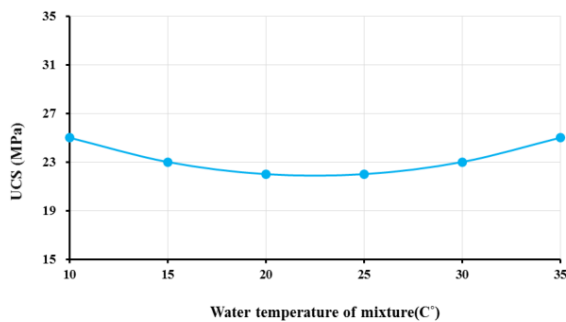

Fig. 4 The effect of water content on UCS

Fig. 5 The effect of water temperature on UCS of small scale samples

As illustrated in Fig. 3, the best mixture was combination of P=40%, C=20% and W=40% with UCS=20.67 MPa. Since one objective of this research was to investigate the effect of joint JRC on the mechanical response of samples, the material needed to have a relatively high strength. Therefore in order to achieve the highest possible UCS, the P/C ratio equal to 2 was obtained. To investigate the effect of water content on the sample strength, four samples with W=30, 35, 40 and 45% were prepared. The effect of water content on UCS is illustrated in Fig. 4.

At W>40%, the UCS was quickly decreased while for W≤35% making the paste was not possible. The optimized value was W=40%. The effect of water temperature of mixture has also been studied on UCS and presented in Fig. 5. It can be concluded that the least changes of uniaxial strength value are corresponded to the temperature interval of 20 to 25C°. In addition, this is about room temperature and comfortable for working.

2.2 The mixture plan for the main blocks

The optimum mixture plan was used to make the main blocks (width 300 mm, height 300 mm and thickness 120 mm). Since the amount of material for each block was high and proper mixing was taking too long, this left a short time for pouring and setting the samples properly. To gain more time, some retarder and lubricant was used. Although retarder increases the gelation time of the mixture, it decreases the unconfined compression strength of the sample. Therefore in order to investigate the effect of retarder on gelation time and UCS for large samples, six samples with different percentage of retarder were made and the relation between gelation time and UCS was recorded (Fig. 6).
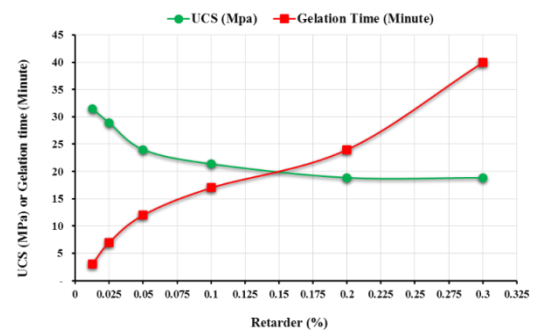

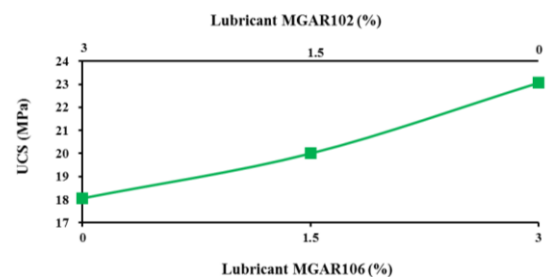Fig. 6 The effect of retarder on gelation time and UCS of samples

Fig. 7 The effect of two different lubricant on the uniaxial compression strength of large scale samples

At least 10 minutes of gelation time was needed for producing large scale samples. Therefore, 0.05 wt% retarder with 12 minutes of gelation time was selected according to Fig. 5. Moreover, the solid content and fluidity of mixture increase as the result of reducing its water content by lubricant. Accordingly, two commercial lubricants, MGAR102 and MGAR106, were investigated in this research. Based on the strength of the relevant company, maximum UCS of sample was obtained using 3% lubricant by weight of plaster content of mixture. Hence, three configurations of the lubricants were tested on large scale samples and presented in Fig. 6. The results showed that using 3% lubricant MGAR106 resulted in the increase of plaster content from 40% to 48.33%, cement content from 20% to 24.17% and decrease of water content from 40 to 27.5%. This all in turn yielded increase of UCS from 6 MPa to 22.97 MPa in block strength.

By using lubricant MGR106 mixing time was reduced from 10 to 4 minutes and water content from 40 to 27.5%. It is worth mentioning that the combination of retarder and MGAR106 factor resulted in extend of the paste gelation time. This is very effective in creating non-persistent mated joints; otherwise, this period decreases to less than 2 minutes (Asadizadeh *et al.* 2016, 2017). Moreover, it is not possible to create mated non-persistent joints with minimum cohesion.

2.3 Mechanical properties of intact samples

Mechanical properties of the artificial material was determined by laboratory tests such as UCS, Triaxial and Brazilian tests on small and large scale samples. A summary of mechanical properties of samples is listed in Table 1.

2.4 The equipment for joined sample preparation

2.4.1 JRC sheets

The joints were planned to be created using 3D JRC sheets with dimension of $150 \times 100 \times 1$ mm (Fig. 8(a)). In order to create 3D JRC sheets, the standard JRC profiles introduced by Barton were digitized using Engauge Digitizer software. The 3D JRC sheets were designed based on the digitized profiles utilizing SolidWorks software. Finally, the designed sheets were produced using a 3D printer (Fig. 8(b)). The mechanical properties of JRC sheets material are presented in Table 2.

2.4.2 The cast for jointed samples

In order to create repeatable samples, a cast was designed to have a high flexibility of making wide range of non-persistent joint parameters. In the samples, the parameters L, γ, JRC and θ need to be variable as depicted in Fig. 9.

A schematic view of the casting assembly is shown in Fig. 10. The cast has made up of three different parts: 1) frame, the combination of a box and upper platform; 2) T shape segment, held by upper platform and connected to L shape segment; and 3) a pair of L shape parts on which JRC sheets are assembled. The components of cast are as follows:

1- The main box: the bottom of the main box and the walls are made of steel and Plexiglas, respectively. They are connected by bolts at the bottom of the box. The dimensions of the box are 300 mm×300 mm×120 mm.

2- Bolt rail: on each wall, a profile has been mounted on which the head of a bolt can easily move. These profiles act as a rail for the bolt. A ruler has also been installed on these profiles to control the joint inclination (θ) utilizing the x-y coordinate system.

3- The upper platform: assembled on the box using two rods.

4- Protractor: installed on the upper platform to control the bridge angle (γ).

5- T segment: there is a hole on the upper platform in which the T segment can easily rotate and measure the rotation along the protractor through a mounted pointer. On the lower part of the T segment as well, there is a sliding rail on which the head of L segment can easily move, and a ruler which controls the length of the bridge.

6- The head of L segment can easily move in the sliding rail of the T segment. This can be fixed by two bolts which are installed in its upper and lower parts. The head and other parts of L segment rotate easily around the lower bolt.

7- The L-segment: it is placed on a sliding rail-like profile and has a notch in its lower part. This segment can easily move in x and y directions using a bolt located on the mentioned rail.

8- The notch: JRC sheet is easily seated in second notch (number 8 in Fig. 10). On top of this notch there is a set of jaws that hold the JRC sheet. Two sets of bolts on the top can fix these jaws.

9- The JRC sheets: these sheets can be held by the lower part of L segments.

Table 1 Mechanical properties of the samples

Parameter	Small specimens	Large specimens
σ_{ci} (MPa)	23.70	21.97
E_i (GPa)	10.53	3.78
σ_t (MPa)	3.43	…
Poisson's ratio	0.17	…
Cohesion (MPa)	10.99	…
Internal friction angle (degrees)	23.95	…

Table 2 Mechanical properties of JRC sheets (All units in MPa)

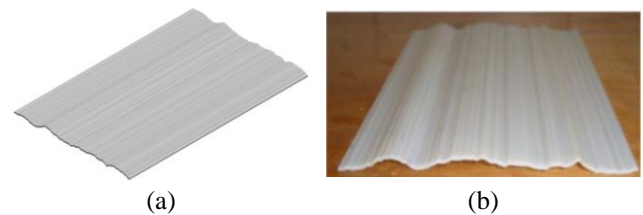| Material	σ_{ci}	E_i	Tensile strength	Flexural strength	Flexural modulus
VeroGray	85.5	3000	60	95	3000

| (a) | (b) |

Fig. 8 3D JRC sheet (JRC=18-20) (a) designed by SolidWorks software and (b) produced using 3D printer
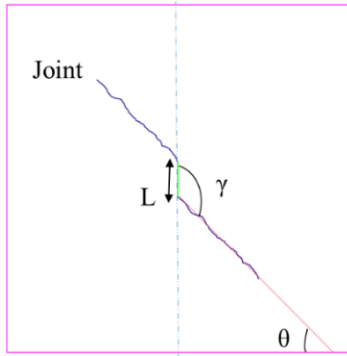
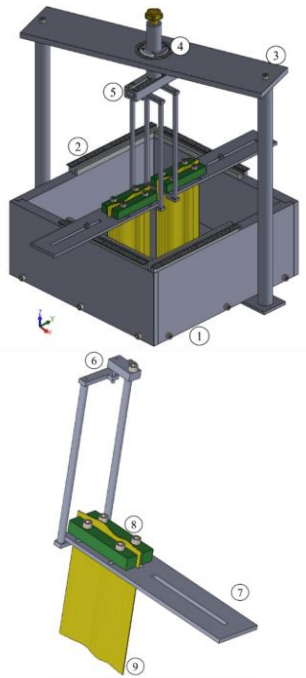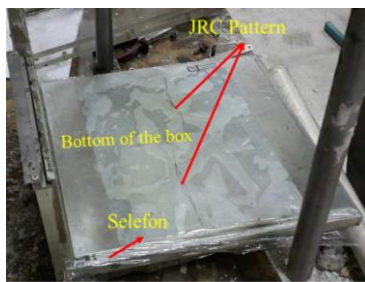Fig. 9 Non-persistent jointed block parameters

Fig. 10 Schematic view of designed cast for precreation of non-persistent jointed samples
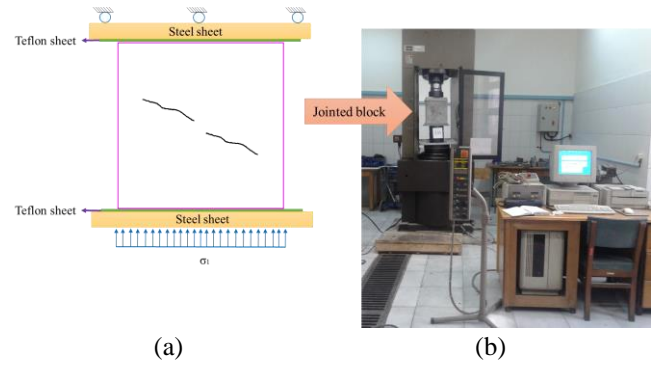

(a)

(b)

Fig. 11 Non-persistent jointed specimen preparation (a) The pattern of joints at the bottom of the cast and (b) Stepped nan-persistent jointed specimen (JRC, 0-2)

(a)   (b)

Fig. 12 (a) UCS sample and its boundary conditions under uniaxial compression test and (b) a view of the MTS testing apparatus

2.5 Sample preparation

In order to produce jointed samples with JRC, extreme care was taken to make sure the JRC sheet is located in the right place and right direction (Fig. 11(a)). After cast regulations the paste was gently poured in the cast. It was very crucial to keep JRC sheets unmoved. In this regard, two actions was necessary simultaneously: 1) the mortar should be poured very slowly and gently from the corners of the cast; 2) applying a normal load on the JRC sheets, until the cast was completely full. The mortar was well mixed for 12 minutes and while hardening, the sheets were removed simultaneously.

The critical part of this process was the removal time of JRC sheets. If the sheets were removed very soon, the joint surfaces might have glued to each other and inherit high cohesion. Besides, if the removal time of the sheets exceeded 12 minutes, the sheets stuck into the sample and could not be removed. Therefore, the sample would be lost. A view of non-persistent joint with JRC 0-2 is illustrated in Fig. 11(b).

2.6 Test setup

The tests were performed using a Material Testing Machine (MTS) under displacement control condition. For the UCS tests, the constant velocity for the actuator head was 0.005 mm/s. The load was applied to the specimen using two steel platens and in order to neutralize the effect of friction between these steel plates and the sample, 2 mm thick Teflon sheets were used for each side. A close view of the MTS testing apparatus, sample parameters and loading condition is illustrated in Fig. 12.

3. Mechanical characteristics of the specimens

In order to investigate the influence of non-persistent joints on the mechanical properties of the samples, the effect of joint inclination (θ), Joint roughness coefficient (JRC), bridge angle (γ) and bridge length (L) on the uniaxial compressive strength and deformation modulus were studied. Therefore, to further understand the relationship between the mechanical response of samples and the

parameters, it is necessary to identify the way in which the coupled effects of the joints influence the response. In order to design the experiments in a way to reduce the number of experiments and taking into account the coupled effect of joint parameters on the responses, the Response Surface Methodology (RSM) was adopted in this research.

Table 3 Independent variable codes and their levels in the CCD experiment

Factor	Code	Level				
		$-\alpha$	-1	0	1	$+\alpha$
Joint Roughness Coefficient	JRC	0	5	10	15	20
L (mm)	L	10.0	17.5	25.0	32.5	40.0
γ (degree)	B.A	90.0	112.5	135.0	157.5	180.0
θ (degree)	J.A	0.0	22.5	45.0	57.5	90.0

3.1 Design of experiments, RSM and CCD

The experimental design methods, such as Response Surface Methodology (RSM), that are combination of statistical and arithmetical approaches, have been developed to model a process and explore the interaction of factors on the response of a system (Kirmizakis *et al.* 2014, Sodeifian 2014, Yuan 2015, Liu 2015). Choosing a suitable model that can evaluate the effect of independent variables and their common influence on dependent variables with the minimum number of experiments is very crucial. RSM can easily cope with small number of experiments to evaluate the interaction amongst variables on the response (Kirmizakis *et al.* 2014, Sodeifian 2014). In this research, a mathematical model was developed utilizing the Design-Expert 7 software. The central composite design (CCD) module was utilized to model RSM. The independent variables included in the modeling process are θ, γ, L, and JRC (Fig. 9). The dependent variables are the uniaxial compressive strength and deformation modulus of the jointed blocks, which can be expressed using a quadratic model as follows (Kirmizakis *et al.* 2014, Liu 2015, Noshadi 2012)

$$y = \beta_0 + \sum_{i=1}^{3} \beta_i X_i + \sum_{i=1}^{3} \beta_{ii} X_i^2 + \sum_{i=1}^{3} \sum_{j=i+1}^{3} \beta_{ij} X_i X_j \quad (1)$$

where y is the response variable representing the compressive strength or deformation modulus of the non-persistent jointed sample; β_{ii}, β_{ij}, β_i, and β_0 are regression coefficients; and X_i and X_j are the values of the independent variables coded in the program that can be expressed as follows

$$X_i = \frac{x_i - x_0}{\Delta x} \quad (2)$$

where x_0 is the value of xi at the center point and Δx is the change step. The code and level of the independent variables in the CCD are presented in Table 3. In this CCD experiment α has taken as equal to 2.

A total CCD experiment contains 30 points. Amongst

them, 24 points are factorial points and 6 points are zero points which are used to estimate the experimental error. The CCD experiment scheme and results are presented in Table 4.

Table 4 CCD experiments and the experimental results

Sample code	JRC	L (mm)	γ (degree)	θ (degree)	σ_{cj} (MPa)	E_j (GPa)
U1	10-12	25.0	135.0	0.0	21.66	4.44
U2	0-2	25.0	135.0	45.0	15.00	3.12
U3	14-16	17.5	112.5	67.5	16.04	3.18
U4	14-16	17.5	157.5	67.5	18.47	3.61
U5	18-20	25.0	135.0	45.0	19.03	3.53
U6	4-6	32.5	157.5	67.5	15.99	3.35
U7	4-6	17.5	157.5	67.5	15.61	3.21
U8	4-6	17.5	112.5	22.5	17.50	3.40
U9	14-16	17.5	157.5	22.5	18.90	4.01
U10	4-6	32.5	112.5	22.5	18.03	3.32
U11	10-12	25.0	135.0	45.0	17.01	3.41
U12	10-12	25.0	135.0	45.0	16.21	3.52
U13	4-6	32.5	157.5	22.5	18.57	3.63
U14	10-12	25.0	180.0	45.0	18.88	3.52
U15	10-12	25.0	135.0	45.0	16.44	3.19
U16	4-6	17.5	112.5	67.5	16.19	3.34
U17	14-16	17.5	112.5	22.5	18.61	3.24
U18	10-12	25.0	135.0	45.0	16.04	3.21
U19	10-12	25.0	135.0	90.0	17.60	3.54
U20	10-12	25.0	90.0	45.0	13.90	3.10
U21	10-12	10.0	135.0	45.0	15.50	3.01
U22	14-16	32.5	112.5	22.5	18.34	4.08
U23	4-6	32.5	112.5	67.5	16.19	2.80
U24	14-16	32.5	112.5	67.5	14.12	3.86
U25	14-16	32.5	157.5	67.5	16.37	4.04
U26	14-16	32.5	157.5	22.5	19.34	4.07
U27	10-12	25.0	135.0	45.0	16.55	3.35
U28	4-6	17.5	157.5	22.5	18.92	3.61
U29	10-12	40.0	135.0	45.0	18.52	3.60
U30	10-12	25.0	135.0	45.0	16.78	3.21

Table 5 Statistical parameter of RSM models

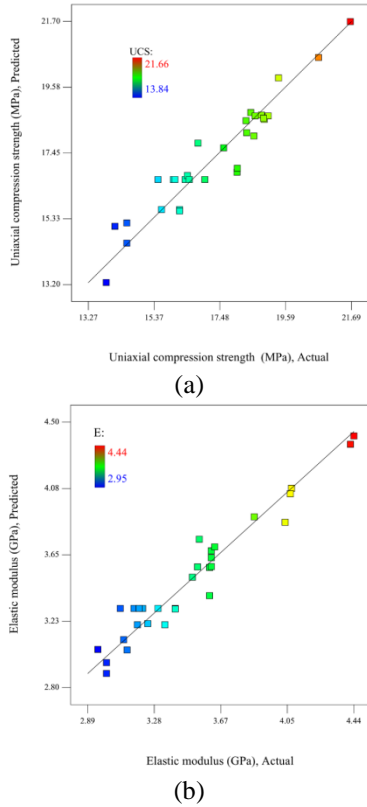| Statistical parameter	UCS Model	Deformation modulus model	Description
F-value	27.79	32.15	Models are significant
Adequate precision	23.70	24.05	Models can be used to navigate the design space
Lack of Fit F-value	2.48	0.61	The lack of fit is not significant.
R^2	0.9444	0.9353	High correlation between the exponential and the predicted values
Adjusted-R^2	0.9104	0.9063	In a good agreement with their R^2 coefficient

(a)

(b)

Fig. 13 The actual and predicted (a) Uniaxial compression strength and (b) Deformation modulus of the non-persistent jointed samples
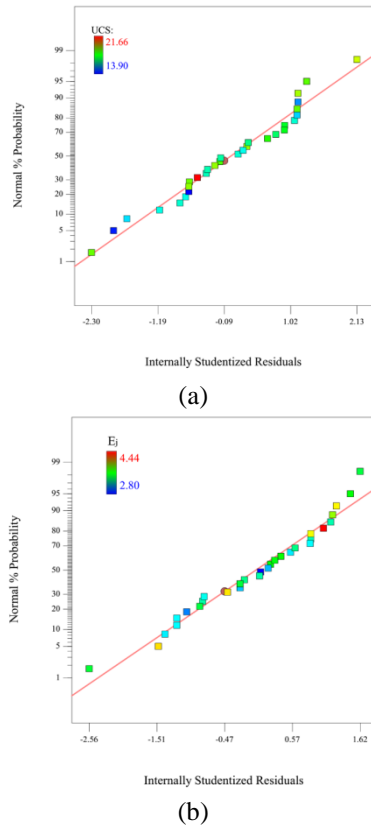

(a)

(b)

Fig. 14 Normal probability plot for the (a) Uniaxial compressive strength and (b) Deformation modulus of the non-persistent jointed samples

3.2 Variance analysis (ANOVA)

The analysis of variance (ANOVA) technique was applied to the results of the RSM design to estimate the contribution of each input parameter and their interactions on the variability of the output responses (Montgomery 2001). The statistical parameters of two models are presented in Table 5.

Based on Table 5 the F-value of models implies they are significant. There is only a 0.01% chance that such a large "Models F-Value" occur due to noise. The "Adeq Precision" measures the signal-to-noise ratio. A ratio greater than 4 is desirable. The "Lack of Fit F-value" implies that the lack of fit compared to the pure error is not significant. For UCS and deformation modulus models, there are 16.22% and 78.86% chance that a "Lack of Fit F-value" becomes significant. These relatively high chances could occur due to noise. For both models, lack of fit was not significant.

In addition, the actual and predicted compressive strength and deformation modulus depicted in Fig. 13(a) and 13(b) shows a linear regression relationship.

The relationship between the normal percentage probability and the studentized residual of both UCS and tangential deformation modulus are depicted in Fig. 14(a) and 14(b) respectively.

A nonlinear pattern (an "S-shaped curve") indicates a non-normality in the error term. In Fig. 14(a) and 14(b), linear dependency is observed, meaning that a response transformation is not needed, nor are there any obvious problems with the normality. All these aforementioned analyses prove that the modified quadratic response models are suitable for the CCD experiment and the prediction of the uniaxial compressive strength and deformation modulus.

3.3 Multiple regression modeling

The polynomial models, functions of the four mentioned joint parameters, were obtained according to the data listed in Table 4. Final equations in terms of coded factors for UCS and deformation modulus are presented as follows

$$
\begin{aligned}
UCS = & 16.62 + 1.01 \times JRC + 0.75 \times L + 1.24 \times \gamma - 1.14 \times \theta - 0.28 JRC \times L - .025 L \times \theta \\
& + 0.74 \times \theta^2 + 0.38 JRC \times \gamma \times \theta - 0.96 JRC^2 L - 0.80 JRC^2 \gamma - 0.81 JRC \times L^2
\end{aligned}
\tag{3}
$$

$$
\begin{aligned}
E = & 3.34 + 0.10 \times JRC + 0.11 \times L + 0.13 \times \gamma - 0.16 \times \theta + 0.15 JRC \times L \\
& + 0.18 \times \theta^2 - 0.11 \times JRC \times L \times \gamma + 0.069 L \times \gamma \times \theta + 0.11 \times JRC \times L^2
\end{aligned}
\tag{4}
$$

According to the Eq. (3), the order of effective independent parameters on UCS was: bridge angle (γ), joint inclination (θ) and JRC. It is worth mentioning that amongst all independent parameters, bridge length (L) had the least influence on UCS. On the other hand, based on the Eq. (4), the order of effective independent parameters on deformation modulus was Joint angle (θ), bridge angle (γ), bridge length (L) and JRC. It should be noted that, in all Figs., JRC is presented in its average level. Except JRCs of 0-2, 10-12 and 18-20 which are presented by 0, 10 and 20 respectively.

4. Results

4.1 Response surface analysis of uniaxial compression strength

To illuminate the influence of joint parameters on the compressive strength, relationship between the dependent variable and one independent variable when the other variables are kept constant at their middle level are depicted in Fig. 15. The influence of JRC on the compressive strength is illustrated in Fig. 15(a) according to which an increase in the JRC increases the compressive strength of the samples. An increase in JRC from category 4-6 to category 14-16 causes 12.94% increase in the compressive strength (from 15.61 MPa to 17.63 MPa). The influence of the bridge length (L) on the compressive strength is plotted in Fig. 15(b). With an increase in the bridge length (L) from 17.5 mm to 32.5 mm, the compressive strength rises from 15.57 MPa to 17.38 MPa by 9.51%. The relationship between the bridge angle and the compressive strength is illustrated in Fig. 15(c). Note that an increase of the bridge angle from 112.5˚ to 157.5˚ leads to an increase of 16.19 % in the compressive strength (from 15.38 MPa to 17.87 MPa). As it is depicted in Fig. 15(d), the variation of UCS versus joint angle (θ) (from 22.5 to 67.5 degree) is nonlinear, showing a decreasing trend in this interval.
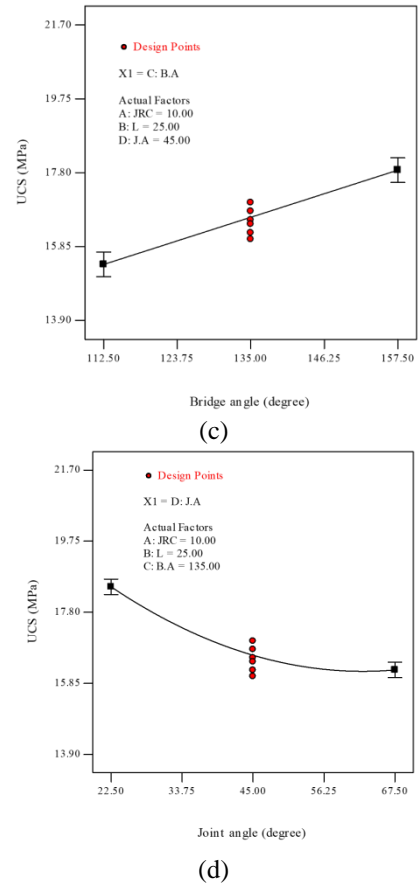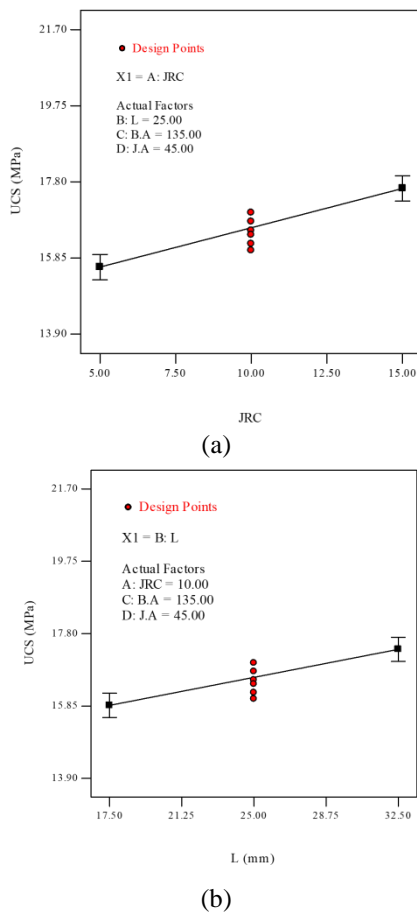

(c)

(d)

Fig. 15 Continued

(a)

(b)

Fig. 15 the influences of (a) JRC, (b) Bridge length, (c) Bridge angle and (d) Joint angle on the uniaxial compressive strength of non-persistent jointed samples

On the other hand, Fig. 16(a) and 16(b) show the influence of bridge length (L) and JRC on the uniaxial compressive strength. As it can be seen in Fig. 16(a) while L is constant, an increase in the JRC has a positive effect on the compressive strength. It is important to note that when L=17.5 mm, an increase in the JRC from category 4-6 to category 14-16 causes 5.81% increase in the compressive strength (from 16.35 MPa to 17.30 MPa); however, when L=32.5 mm, 0.91% decrease is caused by an increase of JRC from category 4-6 to category 14-16 (16.49 MPa-16.34 MPa). Furthermore, when the JRC is constant and located in the category of 4-6, an increase in the bridge length from 17.5 to 32.5 mm causes 0.86% increase in the compressive strength (from16.35 MPa to 16.49 MPa) and when JRC is in category 14-16, the compressive strength decreases by 5.55% (from 17.3 MPa to 16.34 MPa).

Furthermore, Fig. 16(c) and 16(d) show the effect of bridge length (L) and joint angle (θ) on the uniaxial compressive strength. According to Fig. 16(c) and 16(d), while the joint angle (θ) is constant, an increase in the bridge length (L) has a positive effect on the compressive strength. It is important to note that when θ=22.5˚, an increase in the bridge length from 17.5 mm to 32.5 mm causes an 11.49% increase in the compressive strength (from 17.49 MPa to 19.50 MPa); while θ=67.5˚, an increase in the bridge length from 17.5 mm to 32.5 mm causes 6.43% increase in the compressive strength (15.71 MPa-16.72 MPa). Additionally, as it is depicted in Fig. 16(c) and 16(d), while the bridge length is constant, an increase in

(a)

(b)

(c)

(d)

Fig. 16 Response surface and contour plots that represent the effect of two variables and their interaction on the compressive strength of the non-persistent jointed blocks when the other variables are held at their middle levels: (a) and (b) Bride length and JRC (3D surface and interaction plot respectively); (c) and (d) Bridge length and Bridge angle (3D surface and interaction plot respectively); (e) and (f) Bridge angle and JRC (3D surface and interaction plot respectively)
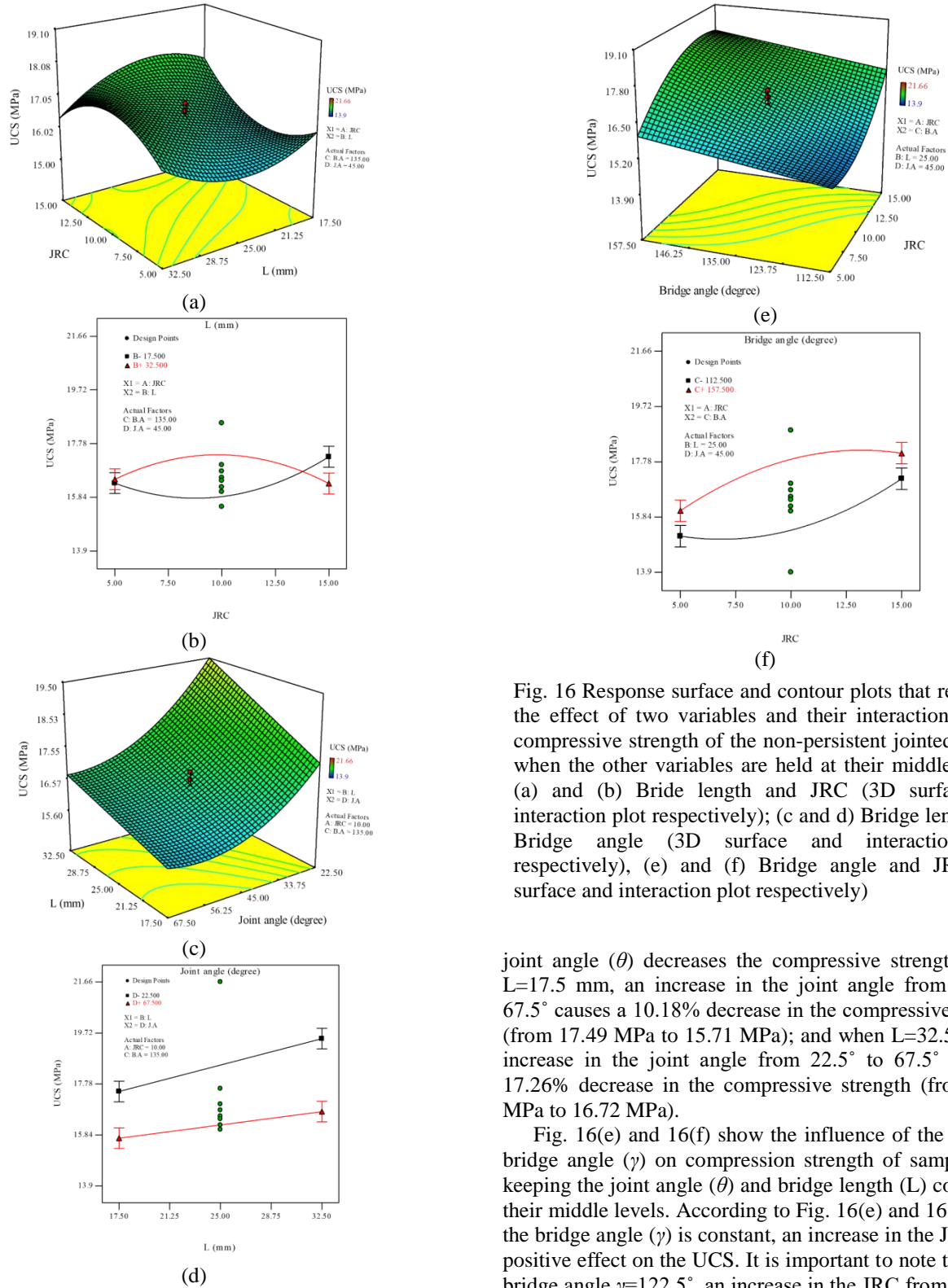

(e)

(f)

Fig. 16 Response surface and contour plots that represent the effect of two variables and their interaction on the compressive strength of the non-persistent jointed blocks when the other variables are held at their middle levels: (a) and (b) Bride length and JRC (3D surface and interaction plot respectively); (c and d) Bridge length and Bridge angle (3D surface and interaction plot respectively), (e) and (f) Bridge angle and JRC (3D surface and interaction plot respectively)

joint angle (θ) decreases the compressive strength. When L=17.5 mm, an increase in the joint angle from 22.5° to 67.5° causes a 10.18% decrease in the compressive strength (from 17.49 MPa to 15.71 MPa); and when L=32.5 mm, an increase in the joint angle from 22.5° to 67.5° causes a 17.26% decrease in the compressive strength (from 19.50 MPa to 16.72 MPa).

Fig. 16(e) and 16(f) show the influence of the JRC and bridge angle (γ) on compression strength of samples with keeping the joint angle (θ) and bridge length (L) constant at their middle levels. According to Fig. 16(e) and 16(f), while the bridge angle (γ) is constant, an increase in the JRC has a positive effect on the UCS. It is important to note that when bridge angle γ=122.5°, an increase in the JRC from category 4-6 to 14-16 causes a 13.25% increase in the UCS (from 15.17 MPa to 17.18 MPa); however, when bridge angle γ=157.5°, 12.55% increase is caused by an increase of JRC from category 4-6 to 14-16 (16.06 MPa-18.08 MPa). This finding implies that an increase in the bridge angle (γ) decreases the capacity of the JRC to weaken the UCS. When the JRC is constant, an increase in the bridge angle (γ) causes an increase in the uniaxial compression strength. When JRC=4-6, if the bridge angle (γ) increases from

112.5˚ to 157.5˚, the UCS increases by 5.87% (from 15.17 MPa to 16.06 MPa), and when JRC=14-16, an increase of the bridge angle (γ) from 112.5˚ to 157.5˚ causes a 5.24% increase in UCS (17.18 MPa-18.08 MPa).
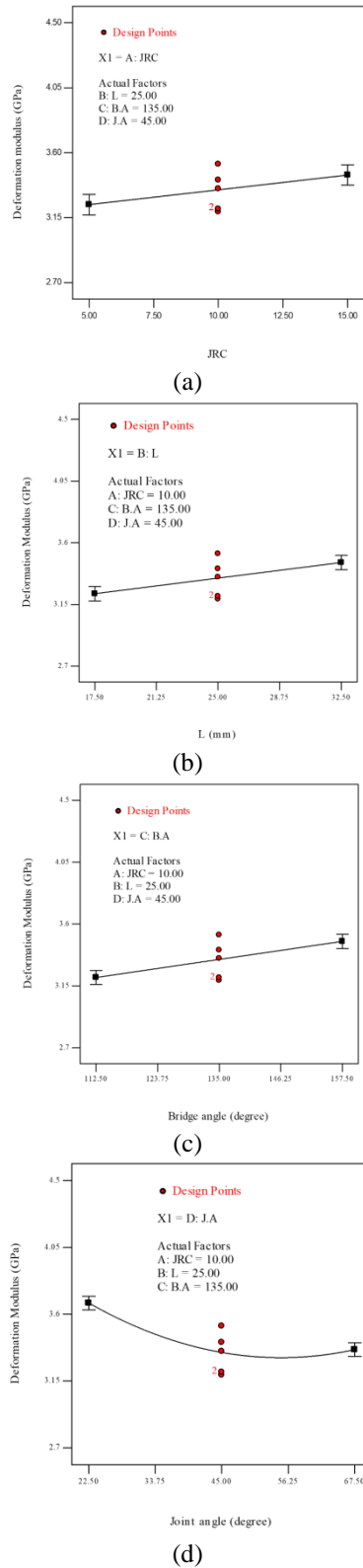

(a)

(b)

(c)

(d)

Fig. 17 The influences of (a) JRC, (b) Bridge length, (c) Bridge angle and (d) Joint angle on the deformation modulus of jointed samples

(a)

(b)

(c)

(d)

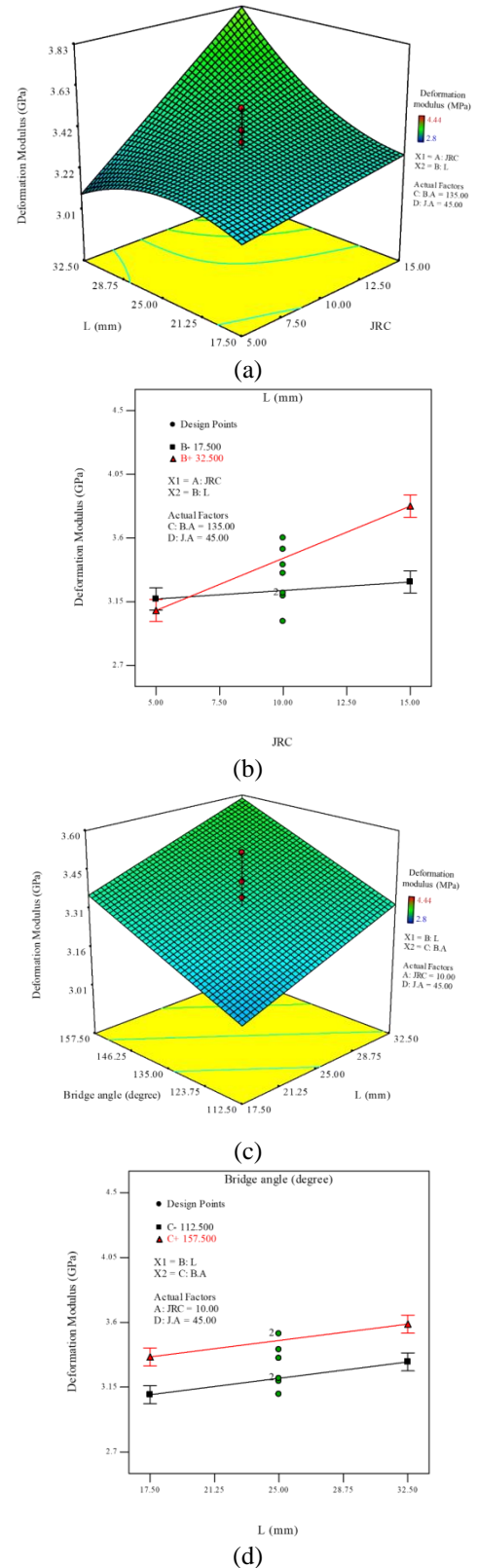Fig. 18 Response surface and contour plots that represent the effect of two variables and their interaction on the compressive strength of the non-persistent jointed specimens when the other variables are at their middle levels: (a) and (b) Bride length and JRC (3D surface and interaction plot respectively), (c) and (d) Bridge angle and bridge length (3D surface and interaction plot respectively)

4.2 Response surface analysis of deformation modulus

To clarify the influences of joint parameters on the deformation modulus of non-persistent jointed rock-like samples, the effect of each independent variable, when the other variables are held constant at the middle level, on deformation modulus are presented in Fig. 17. The influence of JRC on the deformation modulus is illustrated in Fig. 17(a). An increase in JRC increases the deformation modulus of sample. It is important to note that an increase in JRC from category 4-6 to 14-16 causes a 6.48% increase in the response (from 3.24 GPa to 3.45 GPa). The influence of the bridge length on the deformation modulus is plotted in Fig. 17(b). With an increase in the bridge length from 17.5 to 32.5 mm, the response increases from 3.23 GPa to 3.46 GPa by 7.12%. Fig. 17(c) depicts the relationship between the bridge angle and the deformation modulus of samples. An increase in the bridge angle from 112.5° to 157.5° leads to an increase of 8.10% in the deformation modulus (from 3.21 GPa to 3.47 GPa). As it is illustrated in Fig. 17(d), the variation of deformation modulus versa joint angle (θ) is nonlinear and an increase of the joint angle from 22.5° to 67.5° leads to a decrease of 8.70% in the deformation modulus (from 3.68 GPa to 3.36 GPa).

To elucidate the coupling effect of joint parameters on the deformation modulus, 3D surface and interaction plots of the relationship between the dependent variable and two independent variables, again with other variables being constant at their middle levels, are depicted in Fig. 18.

Fig. 18 Response surface and contour plots that represent the effect of two variables and their interaction on the compressive strength of the non-persistent jointed specimens when the other variables are at their middle levels: (a and b) Bride length and JRC (3D surface and interaction plot respectively); (c and d) Bridge angle and bridge length (3D surface and interaction plot respectively).

Fig. 18(a) and 18(b) show the influence of the bridge length (L) and JRC on the deformation modulus when the bridge angle (γ) and joint angle are held at their middle levels. Fig. 18(a) shows, while the bridge length (L) is constant, an increase in the JRC has a positive effect on the deformation modulus. When L=17.5 mm, an increase in the JRC from category 4-6 to 14-16 causes a 3.82% increase in the deformation modulus (from 3.17 GPa to 3.29 GPa); however, when L=32.5 mm, 23.89% increase is caused by an increase of JRC from category 4-6 to 14-16 (3.09 GPa-3.83 GPa). When the JRC is constant, an increase in the bridge length causes fluctuation in the deformation modulus. When JRC is in category 4-6, if the bridge length increases from 17.5 to 32.5 mm, the deformation modulus will decrease by 2.56% (from 3.17 GPa to 3.09 GPa), and when JRC is in category 14-16, an increase of the bridge length from 17.5 to 32.5 mm leads to a 16.31% increase in the deformation modulus.

Fig. 18(c) and 18(d) show the influence of the bridge angle (γ) and bridge length (L) on the deformation modulus when the JRC and joint angle are kept at their middle levels. Fig. 18(c) and 18(d) show while the bridge angle is constant, an increase in the bridge length has a positive effect on the deformation modulus. It is important to note

that when γ=112.5°, an increase in the bridge length from 17.5 to 32.5 mm causes a 7.34% increase in the deformation modulus (from 3.10 GPa to 3.33 GPa); however, when γ=157.5°, 6.77% increase is caused by an increase of bridge length from 17.5 to 32.5 mm (3.36 GPa-3.59 GPa). This finding implies that an increase in the bridge angle decreases the capacity of the bridge length to weaken the deformation modulus. When the bridge length is constant, an increase in the bridge angle causes an increase in the deformation modulus. When L=17.5 mm, an increase of γ from 112.5° to 157.5°, increases deformation modulus by 8.74% (from 3.10 GPa to 3.36 GPa), and when L=32.5 mm, an increase of γ from 112.5° to 157.5° causes a 7.89% increase in the deformation modulus (from 3.33 GPa to 3.59 GPa).

(a)

(b)

(c)

Fig. 19 The effect of bridge angle on its failure mode (a) U20 (γ=90°, tensile), (b) U12 (γ=135°, shear-tensile) and (c) U14 (γ=180°, shear)

(a)

(b)

(c)

Fig. 20 Asperity "interlocking crack" concept (a) U23 (JRC 4-6, no interlocking crack), (b) U20 (JRC 10-12, shear-tensile interlocking crack) and (c) U5 (JRC 18-20, shear-tensile interlocking crack)

5. Discussion

Mechanical behavior of non-persistent jointed blocks containing two parallel, both coplanar and stepped, close and rough non-persistent joints that are subjected to uniaxial compression has been examined by the physical modeling. The influence of the joint roughness coefficient (JRC), bridge length (L), bridge angle (γ) and joint inclination (θ) on the uniaxial compression strength and deformation modulus is elaborated below.

Based on the results of response surface method

(RSM), an increase in JRC (while other parameters are kept constant at their average levels), increases the uniaxial strength and deformation modulus of samples. This could be due to interlocking of asperities and increasing resistance force against shearing on the joint surface. Similarly, an increase in bridge length (L) intensifies UCS and deformation modulus of the samples. When bridge length increases, the load bearing area in the bridge increases; therefore, UCS and deformation modulus rise accordingly (Figs. 15(b) and 17(b)). The result of this study on the effect of bridge angle, is in high agreement with the results of literature (Yang *et al.* 2015, Huang *et al.* 2015, Wong and Einstein 2008, Park and Bobet 2009, Lee and Jeon 2011). The results show that the failure mode of rock bridge in the interval of $\gamma=90°$ to $\gamma=180°$ changes from pure tension to pure shear. (Fig. 19). As illustrated in Fig. 19(a), when $\gamma=90°$ (sample U20), the bridge fails under pure tension and when $\gamma=135°$ (sample U12), the bridge fails under mixed mode of shear-tension (Fig. 19(b)). Consequently, by increasing γ to $180°$ (sample U14), the bridge fails under pure shear condition (Fig. 19(c)).

By increasing the bridge angle, UCS and deformation modulus increase. On the other hand, by increasing joint angle from $\theta=22.5$ to $\theta=67.5°$, UCS and deformation modulus decrease. There is a high agreement between the results of this study and previous findings in this area. In addition, the interaction between JRC and bridge length affects UCS and deformation modulus (Figs 16(a) and 18(a)). It should be noted that in high stress, asperity interlock during loading stage can trigger mixed mode cracks that usually initiate in shear and continue in tensile condition. This type of cracks are called 'interlocking cracks', which can happen when JRC increases, (Fig. 20(a) and 20(b)). Contrary to this, in lower JRC, 'interlocking cracks' cannot progress (Fig. 20(c)). Initiation and propagation of this type of cracks can reduce mechanical properties of sample before reaching its peak strength.

Therefore, when JRC is between categories 10-12 and 18-20 the interlocking of asperities finally leads to initiation and propagation of 'interlocking cracks'. On the other hand, when bridge length is high, bridge fails at higher stress amounts. Therefore, in high bridge lengths, initiation of interlocking cracks before the sample reaches the peak strength, affects UCS and deformation modulus and reduces the mechanical behavior of sample. Moreover, the interaction between JRC and bridge angle is somehow similar to that between JRC and bridge length (Fig. 16(e)). As discussed above, in high of bridge angle (i.e., $\gamma=180°$), shearing in the rock bridge is predominant. Furthermore, in JRCs more than category 10-12, 'interlocking cracks' can weaken the mechanical properties of sample. Therefore, in high levels of JRC and bridge angle, 'interlocking cracks' can reduce the UCS and deformation modulus for non-persistent rough jointed sample

6. Conclusions

The results of laboratory studies and RSM method showed that the rock bridge had a significant effect on mechanical behaviour of non-persistent jointed blocks.

Different bridge parameters had different effects on mechanical response of sample. The most effective independent parameter on UCS was bridge angle (γ), while bridge length (L) was the least important one. For the deformation modulus, joint angle (θ) was the most and JRC was the least effective parameters. The following key conclusions can also be drawn.

1. Increasing JRC, bridge length or bridge angle, while other parameters were held constant, increases UCS and deformation modulus. The effect of these parameters on deformation modulus was much less than that of UCS.

2. Increasing the joint inclination form 22.5° to 67.5° decreased UCS and deformation modulus.

3. The interaction of JRC and bridge length (L) on deformation modulus showed a direct relation with JRC for any bridge length values. However, at lower level of bridge length UCS increased while at its upper level, UCS decreased as a function of JRC.

4. For lower limit of JRC, bridge length had little effect on UCS and deformation modulus. At higher JRC values, with increasing bridge length (L), UCS decreased and deformation modulus increased.

5. Interaction of joint angle with bridge length showed that in all levels of joint angle with increasing bridge length, UCS increased. Moreover, in all L values, an increase in the joint angle, reduced UCS.

6. The interaction of bridge angle and JRC showed while the bridge angle was constant, an increase in JRC had a positive effect on UCS and when JRC was constant, an increase in the bridge angle caused an increase in the uniaxial compression strength.

7. The interaction of bridge length and JRC showed while the bridge length was constant, an increase in the JRC had a positive effect on deformation modulus and when JRC was constant, an increase in the bridge length caused fluctuations in the deformation modulus.

8. In high stress levels, asperity interlocking during loading stage can trigger mixed mode cracks that usually initiates in shear and continues in tensile mode. This type of cracks are called 'interlocking cracks', which can happen when JRC increases, In contrast, in lower JRC, 'interlocking cracks' cannot progress. Initiation and propagation of this type of cracks can reduce mechanical properties of sample before reaching its peak stress.

References

Amadei, B. and Goodman, R.E. (1981), "A 3-D constitutive relation for fractured rock masses", *Stud. Appl. Mech.*, **5**, 249-268.

Asadizadeh, M., Hossaini, M.F., Moosavi, M. and Mohammadi, S. (2016), "A laboratory study on mix design to properly resemble a jointed brittle rock", *J. Min. Geoeng.*, **50**(2), 201-210.

Asadizadeh, M., Moosavi, M., Hossaini, M.F. and Masoumi, H. (2017), "Shear strength and cracking process of non-persistent jointed rocks: An extensive experimental investigation", *Rock Mech. Rock Eng.*, 1-14.

Asadollahi, P., Invernizzi, M.A., Addotto, S. and Tonon, F. (2010), "Experimental validation of modified Barton's model for rock fractures", *Rock Mech. Rock Eng.*, **43**(5), 597-613.

Ashby, M.F.A. and Hallam, S.D. (1986), "The failure of brittle solids containing small cracks under compressive stress states", *Acta Metallurgica*, **34**(3), 497-510.

Bahaaddini, M., Hagan, P., Mitra, R. and Hebblewhite, B.K. (2016a), "Numerical study of the mechanical behavior of nonpersistent jointed rock masses", *J. Geomech.*, **16**(1), 04015035.

Bahaaddini, M., Hagan, P.C., Mitra, R. and Hebblewhite, B.K. (2015), "Parametric study of smooth joint parameters on the shear behaviour of rock joints", *Rock Mech. Rock Eng.*, **48**, 923-940.

Bahaaddini, M., Hagan, P.C., Mitra, R. and Hebblewhite, B.K. (2014a), "Scale effect on the shear behaviour of rock joints based on a numerical study", *Eng. Geol.*, **181**, 212-223.

Bahaaddini, M., Saymontry, J., Masoumi, H. and Hagan, P. (2014), "Experimental study of the shear behavior of rock joints under constant normal load and constant normal stiffness conditions", *Proceedings of the 48th US Rock Mechanics/Geomechanics Symposium*, Minneapolis, U.S.A., June.

Bahaaddini, M., Sharrock, G. and Hebblewhite, B.K. (2013b), "Numerical investigation of the effect of joint geometrical parameters on the mechanical properties of a non-persistent jointed rock mass under uniaxial compression", *Comput. Geotech.*, **49**, 206-225.

Bahaaddini, M., Sharrock, G., Hebblewhite, B.K. and Mitra, R. (2012), "Statistical analysis of the effect of joint geometrical parameters on the mechanical properties of non-persistent jointed rock masses", *Proceedings of the 46th US Rock Mechanics Geomechanics Symposium (ARMA)*, Chicago, U.S.A., June.

Cording, E.J. and Jamil, S.M. (1997), "Slide geometries on rock slopes and walls", *Proceedings of the 4th South American Congress on Rock Mechanics*, Santiago, Chile, May.

Einstein, H.H., Veneziano, D., Baecher, G.B. and O'Reilly, K.J. (1983), "The effect of discontinuity persistence on rock slope stability", *J. Rock Mech. Min. Sci.*, **20**(5), 227-236.

Ghazvinian, A., Nejati, H.R., Sarfarazi, V. and Hadei, M.R. (2013), "Mixed mode crack propagation in low brittle rock-like materials", *Arab. J. Geosci.*, **6**(11), 4435-4444.

Ghazvinian, A., Sarfarazi, V., Schubert, W. and Blumel, M. (2012), "A study of the failure mechanism of planar non-persistent open joints using PFC2D", *Rock Mech. Rock Eng.*, **45**(5), 677-693.

Grasselli, G. (2006), "Manuel rocha medal recipient shear strength of rock joints based on quantified surface description", *Rock Mech. Rock Eng.*, **39**(4), 295-314.

Huang, D., Cen, D., Ma, G. and Huang, R. (2015), "Step-path failure of rock slopes with intermittent joints", *Landsl.*, **12**(5), 911-926.

Huang, Y.H., Yang, S.Q., Tian, W.L., Zeng, W. and Yu, L.Y. (2015), "An experimental study on fracture mechanical behavior of rock-like materials containing two unparal-lel fissures under uniaxial compression", *Acta Mech. Sinica*, **32**(3), 442-455.

Jade, S. and Sitharam, T. (2003), "Characterization of strength and deformation of jointed rock mass based on statistical analysis", *J. Geoemech.*, **3**(1),43-54

Jamil, S.M. (1992), "Strength of non-persistent rock joints". Ph.D. Dissertation, University of Illinois, Urbana, Illinois, U.S.A.

Jennings, J.E. (1970), "A mathematical theory for the calculation of the stability of open cast mines", *Proceedings of the Symposium on Theoretical Background to the Planning of Open Pit Mines*, Johannesburg, South Africa, August-September.

Kirmizakis, P., Tsamoutsoglou, Kayan, B. and Kalderis, D. (2014), "Subcritical water treatment of landfill leachate: Application of response surface methodology", *J. Environ. Manage.*, **146**, 9-15.

Lajtai, E.Z. (1969a), "Shear strength of weakness planes in rock", *J. Rock Mech. Min. Sci.*, **6**(5), 499-515.

Lajtai, E.Z. (1969b), "Strength of discontinuous rocks in direct

shear", *Geotechnique*, **19**(2), 218-332.

Lee, H. and Jeon, S. (2011), "An experimental and numerical study of fracture coalescence in pre-cracked specimens under uniaxial compression", *J. Solid. Struct*., **48**(6), 979-999.

Liu, T., Lin, B., Zheng, C., Zou, Q., Zhu, C. and Yan, F. (2015), "Influence of coupled effect among flaw parameters on strength characteristic of precracked specimen: Application of response surface methodology and fractal method", *J. Nat. Gas Sci. Eng*., **26**, 857-866.

Mas Ivars, D., Pierce, M.E., Darcel, C., Reyes-Montes, J., Potyondy, D.O., Young, R.P. and Cundall, P.A. (2011), "The synthetic rock mass approach for jointed rock mass modelling", *J. Rock Mech. Min. Sci*., **48**(2), 219-244.

Montgomery, D. (2001), *Design and Analysis of Experiments*, John Wiley and Sons, New York, U.S.A.

Mughieda, O., Alzo'ubi, A.K. (2004), "Fracture mechanisms of offset rock joints-a laboratory investigation", *Geotech. Geol. Eng*., **22**(4), 545-562.

Noshadi, I., Amin, N.A.S. and Parnas, R.S. (2012), "Continuous production of biodiesel from waste cooking oil in a reactive distillation column catalyzed by solid heteropolyacid: Optimization using response surface methodology (RSM)", *Fuel*, **94**, 156-164.

Park, C.H. and Bobet, A. (2009), "Crack coalescence in specimens with open and closed flaws: A comparison", *J. Rock Mech. Min. Sci*., **46**(5), 819-829.

Prudencio, M. (2009), "Study of the strength and failure mode of rock mass with non-persistent joints", Ph.D. Dissertation, Catholic University of Chile, Santiago, Chile.

Prudencio, M. and Jan, M.V.S. (2007), "Strength and failure modes of rock mass models with non-persistent joints", *J. Rock Mech. Min. Sci*., **44**(6), 890-902.

Saeb, S. and Amadei, B. (1992), "Modelling rock joints under shear and normal loading", *J. Rock Mech. Min. Sci*., **29**(3), 267-278.

Serrano, A., Olalla, C. and Galindo, R.A. (2014), "Micromechanical basis for shear strength of rock discontinuities", *J. Rock Mech. Min. Sci*., **70**, 33-46.

Sherpa, M.D., Hagan, P. and Masoumi, H. (2013), "The effect of joint frequency on a discontinuous rock mass under experimental compressive strength testing conditions", *Proceedings of the 47th US Rock Mechanics Geomechanics Symposium (ARMA)*, San Francisco, California, U.S.A., June.

Sodeifian, G., Azizi, J. and Ghoreishi, S.M. (2014), "Response surface optimization of smyrnium cordifolium noiss (SCB) oil extraction via supercritical carbon dioxide", *J. Supercrit. Fluid*., **95**, 1-7.

Van Sint Jan, M. and Prudencio, M. (2003), "Strength of model rock masses with discontinuous joints", *Proceedings of the 10th Congress of International Society of Rock Mechanics*, Sandton, South Africa, September.

Wang, T.T. and Huang, T.H. (2009), "A constitutive model for the deformation of a rock mass containing sets of ubiquitous joints", *J. Rock Mech. Min. Sci*., **46**(3), 521-530.

Wong, L.N.Y. and Einstein, H.H. (2008), "Crack coalescence in molded gypsum and carrara marble: Part 1. Macroscopic observations and interpretation", *Rock Mech. Rock Eng*., **42**(3), 475-511.

Yang, S., Tian, W.L., Huang, Y.H., Ranjith, P.G. and Ju, Y. (2015), "An experimental and numerical study on cracking behavior of brittle sandstone containing two non-coplanar fissures under uniaxial compression", *Rock Mech. Rock Eng*., **49**(4), 1497-1515.

Yuan, Z., Yang, J., Zhang, Y. and Zhang, X. (2015), "The optimization of air-breathing micro direct methanol fuel cell using response surface method", *Energy*, **80**, 340-349.

Zhang, L. (2010), "Estimating the strength of jointed rock masses", *Rock Mech. Rock Eng*., **43**(4), 391-402.

CC